Desalination and Water Treatment
www.deswater.com

doi: 10.1080/19443994.2013.841101

53 (2015) 398–412
January

Taylor & Francis
Taylor & Francis Group

Detection of Hg(II) amidst several heavy and toxic metal ions after their selective separation by chromatography: rationalization of separation factors in terms of Density Functional (hardness) Index

Bhavya Srivastava, Milan K. Barman, Bhabatosh Mandal*

Department of Chemistry, Visva-Bharati University, Santiniketan, 731235, India
Tel. +91 3463 264935; Fax: +91 3463 261526; +91 9474738517; email: bhabatosh_mandal@yahoo.co.in

Received 18 March 2013; Accepted 26 August 2013

ABSTRACT

Ascending paper chromatography of Hg^{+2} has been performed with mixed acids as developing mobile phase. Effects of temperature, concentration, and composition of the mobile phase on R_f values have been investigated. Hg^{+2} has been selectively separated from several synthetic binary and multicomponent mixtures containing the toxic and heavy metal ions. Often these metal ions remain associated with it in its ores and alloy samples. Hg^{+2} in trace level has been separated and detected from blood serum containing the congeners Zn^{+2}, Cd^{+2}, Pb^{+2}, Bi^{+3}, Th^{+4}, Tl^{+3}, and Cu^{+2}. On the basis of the difference in the migration of the spots on the paper, twenty difficult separations have been achieved. Several thermodynamic parameters, ΔG, ΔH, and ΔS have been determined by differential variation of radii of the spot with respect to temperature utilizing the thermodynamic relationship. The partition equilibrium constant was also determined. Metal ions were detected by borohydride reduction on the paper strip. Separation factors have been correlated in terms of DesityFunctional (corrected hardness, η^*) Index. From η^*, hydrated radii of the metal ions have been determined. A plausible mechanism for the differential migration of diverse metal ions has been suggested.

Keywords: Hg(II); Paper chromatography; Selectivity factor; Hydrated radii; Sorption energy; Hardness index

1. Introduction

Mercury is a heavy and relatively rare element, but it is well known because of its multivariate technical importance as well as its detrimental effects. It is used in thermometers, barometers, mercury vapor lamps, in electrical devices, as an amalgam with other metals in dental fillings, in manufacturing some drugs, paints, and explosives, and by hatters and furriers [1]. Mercury compounds have been used as catalysts, fungicides, herbicides, disinfectants, pigments and for other purposes. The world production was about 10,000 tonnes in 1973 [2] and about 6,500 tonnes in 1980 [3]. In addition to the production of pure mercury by industrial processes, mercury is released into the environment by human activities such as the combustion of fossil fuels, waste disposal and by industry. Recent estimates of anthropogenic emissions are in the order of 2,000–3,000 tonnes per year [4]. Mercury and its compounds are considered

*Corresponding author.

health hazards, and reports of Hg poisoning because of industrial, agricultural, and laboratory exposure as well as its suicidal/homicidal uses are numerous. Persons concerned are liable to get poisoned during fingerprinting by gray powder (hydrargyrum cum creta that contain 30% mercury), mining and in deadening during the manufacturing of mercurial ointment and emplastrum [1]. Mercury accumulated in the tissues of fish is usually in the form of methylmercury, a highly toxic form. Along with massive human intoxication at Minamata, Japan, and in Iraq, new mercury pollution cases in developing countries have resulted from the use of amalgamation in gold mining and changes of chemical form in the environment have been reported [5]. Thus, from this toxicological point of view, separation and detection of mercury in all its forms at micro level is warranted. However, absorption spectroscopy [6], neutron activation analysis [7], anode stripping voltametry [8], colorimetry [9], potentiometry [10], laser-induced plasma spectroscopy [11], are the most effective and accurate methods for the detection of mercury in trace level, but these are very much sophisticated, costly and not affordable in developing countries. Heavy metals have been separated from mercury in their multicomponent synthetic mixtures using extraction chromatography [12–14], but selective eluents are required for each metal ions and these varied for different mixtures of metal ions, as well. Mercury has been separated from binary mixtures by paper chromatography using organic solvents as one of the components [15–20], but these methods are not selective in the presence of chemically correlated congeners of multicomponent versatile systems and the metal ions are not detected by a unique detector. Moreover, the separation factors (R_f values or selectivity factors) in linear solvation free-energy relationships (LSERs) based on the solvatochromic parameters [20], plate theory [21], rate theory [22] and Kielland [23], affinity order have not been quantitatively correlated with any Density Functional Index. Global hardness is a definite quantum mechanical descriptor and it is the cardinal index of chemical reactivity as well as stability of atoms and ions [24]. Paper chromatography is as an effective alternative, when the metals are in large volumes of relatively low concentrations [15]. The present paper reports the systematic investigation for the selective separation and detection of mercury from several synthetic multicomponent mixtures containing toxic and heavy metal ions like Zn^{+2}, Cd^{+2}, Pb^{+2}, Bi^{+3}, Th^{+4}, Tl^{+3}, Cu^{+2}, Fe^{+3}, Co^{+2}, and Ni^{+2}, associated with it in ores and alloy samples by paper chromatography utilizing a unique mobile phase. It is an inexpensive and powerful analytical tool that requires very small quantities of material usually present in real samples. Sorption energy, acid–base-binding energy and hydrated radii in solution phase have been calculated from Density Functional Index. After separation, in most of the cases the detection of mercury and other metal ions have been performed by the single detector, borohydride.

2. Experimental

2.1. Apparatus

Chromatographic paper (Whattman 1), 23×1.5 cm and 28×6 cm chromatography glass jar and pH meter (Digital Elico LI-120, India).

2.2. Test solutions

Standard aqueous (10^{-2} M) of nitrate, sulfate, and chloride of Hg^{+2}, Pb^{+2}, Cu^{+2}, Cd^{+2}, Bi^{+3}, Al^{+3}, Fe^{+3}, Cr^{+3}, Ni^{+2}, Co^{+2}, Zn^{+2}, Mn^{+2}, In^{+3}, Tl^{+3}, and VO^{+2} were used for the present work.

2.3. Mobile phase

Different acid solutions (H_2SO_4, HNO_3, CH_3COOH, HCl, and $HClO_4$) of different concentrations and CH_3COCH_3 were mixed in different proportions to have the suitable mobile phase for clean separation of Hg^{+2} in multicomponent synthetic and real samples (Table 1).

2.4. Detection

Colored metals (Hg^{+2}, Pb^{+2}, Cu^{+2}, Cd^{+2}, Bi^{+3}, Fe^{+3}, Cr^{+3}, Ni^{+2}, Co^{+2}, Mn^{+2}, In^{+3}, Tl^{+3}, and VO^{+2}) were detected by sodium borohydride reduction (E. Merc, Bombay, India), and in other cases, Al^{+3}, Zn^{+2} were detected by xelynol orange (BDH, Bombay, India) as indicator.

2.5. Procedure

Test solutions (spiked or un-spiked metal ion solutions) were spotted separately on paper strip (in μg) using micro capillary about 2 cm above the lower edge of the paper strip. The spots were-air dried (precaution was taken to minimize spreading of applied spots by frequent drying in air) and then the paper strip developed in the chromatographic glass jars with chosen mobile phase by the ascending technique up to the ascent of 20 cm from its point of application. After development, the chromatograms were taken off and air-dried. The positions of the

Table 1
Mobile phases of different compositions

Symbol	Composition
One-component system	
M_1	0.1 M HCl
M_2	0.2 M HCl
M_3	0.5 M HCl
M_4	1 M HCl
M_5	0.01 M H_2SO_4
M_6	0.02 M H_2SO_4
M_7	0.04 M H_2SO_4
M_8	0.5 M H_2SO_4
M_9	0.005 M HNO_3
M_{10}	0.05 M HNO_3
M_{11}	0.2 M HNO_3
Two-component system	
M_{12}	1 M HCl + 10 mL acetone
M_{13}	1 M HCl + 20 mL acetone
M_{14}	1 M HNO_3 + 20 mL acetone
M_{15}	2 M HNO_3 + 20 mL acetone
M_{16}	0.01 M HNO_3 + 20 mL acetone
M_{17}	0.01 M HNO_3 + 40 mL acetone
M_{18}	0.01 M HNO_3 + 60 mL acetone
M_{19}	0.01 M HNO_3 + 100 mL acetone
M_{20}	0.5 M H_2SO_4 + 0.1MCH_3COOH
M_{21}	0.5 M H_2SO_4 + 0.2MCH_3COOH
M_{22}	0.1 M H_2SO_4 + 0.3MCH_3COOH
M_{23}	0.1 M H_2SO_4 + 1 MCH_3COOH
Three-component system	
M_{24}	1 M HNO_3 + 1M CH_3COOH + 40 mL acetone
M_{25}	0.1 M H_2SO_4 + 1MCH_3COOH + 10 mL acetone
M_{26}	0.1 M H_2SO_4 + 1MCH_3COOH + 20 mL acetone
M_{27}	0.1 M H_2SO_4 + 1MCH_3COOH + 40 mL acetone
M_{28}	1 M H_2SO_4 + 1MCH_3COOH + 50 mL acetone
Four-component system	
M_{29}	0.1 MHCl + 0.1M H_2SO_4 + 0.1 M HNO_3 + 0.1MCH_3COOH

analytes were detected using suitable detectors. The R_f values and the selectivity factors (α) for individual analytes were determined. For the separation of Hg^{+2}, equal volumes of metal ion solutions were mixed and was taken (in μg) on the paper strip. The paper strip was developed with suitable mobile phase, and the R_f values were determined. The areas of spot on the Chromatogram of Hg^{+2} at different temperatures were determined for the investigation of different thermodynamic parameters (ΔG, ΔH, and ΔS).

2.6. Analysis of real samples

(i) Different ternary mixtures of Hg^{+2} containing toxic metal ions (Pb^{+2}, Cu^{+2}, Cd^{+2}, Bi^{+3}, Fe^{+3}, Cr^{+3}, Ni^{+2}, Co^{+2}, Mn^{+2}, In^{+3}, Tl^{+3}, and VO^{+2}) in raw water (well, pond, and tap) were prepared for their separation. (ii) In view of the forensic serological sample analysis, human blood samples were collected from pathological laboratory (PM Hospital, Visva-Bharati, India). Hg^{+2} and two other metal ions (such as Pb^{+2}, Cu^{+2}, Cd^{+2}, Bi^{+3}, Zn^{+2}, Co^{+2}, Mn^{+2}, In^{+3}, Tl^{+3}, and VO^{+2}) were added in to the blood samples to prepare different ternary mixtures. The blood samples were then digested with 1:1 HNO_3 and centrifuged at room temperature with the help of Laboratory Centrifuge (REMI R-4C DX,) at 10,000 rpm for 10 min to obtain the metal containing blood serum. The supernatants (blood serum) were collected in small vials, and the separation of Hg^{+2} in different ternary mixtures were obtained on chromatogram. The water samples (pond, well, and tap) were collected using a long glass tube from different places of Santiniketan, Birbhum District, West Bengal, India (24˚32´30´´N-24˚35´´N and 87˚01´´-87˚05´2´´E), and different multi-component mixtures were prepared by adding metallic toxicant. The samples were stored in sample vials. Unless otherwise stated, all chemicals and solvents used in this work were of analytical grade (BDH/E Merck).

3. Results and discussion

3.1. SEM analysis

Scanning electron microscopy (SEM) images of the exchanger (cellulose paper, for both unloaded and loaded with Hg(II)) were taken by SEM-S-530 Hitachi, Japan using Image Management System Software of Quartz PCI Version, shown in Fig. 1. The paper strips and its loaded form were kept in vacuum for 2 min and placed for gold coating in an ion coater, IB-2 (EIKO Engineering, Hitachi, Japan) to prevent any burning during its analysis. The photograph confirms that the material is porous (Fig. 1(a)). After reduction of the spot on the developed chromatogram with borohydride (Fig. 1(b)), the metallic Hg was found to be present inside the pores of the exchanger. Here, the exchanger matrix consists of large number of pores connected by channels. Sieve action of these channels combined with surface adsorption activity of the matrix make it possible to separate the species smaller/bigger than the size of the channels.

3.2. Effect of the nature of mobile phases on R_f values and selectivity factors

Chromatography of ten metal cations was performed using mono- and multicomponent mobile-phase system (M_1–M_{29}), and the mobility pattern of

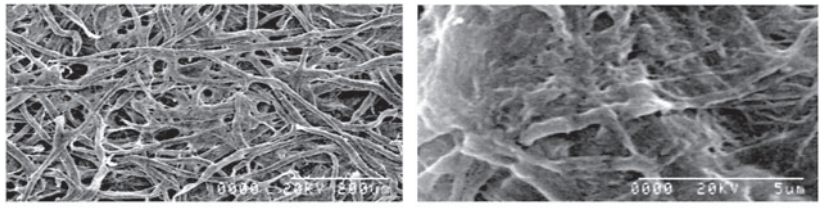

Low resolution High resolution

(a) SEM image of pure cellulose paper

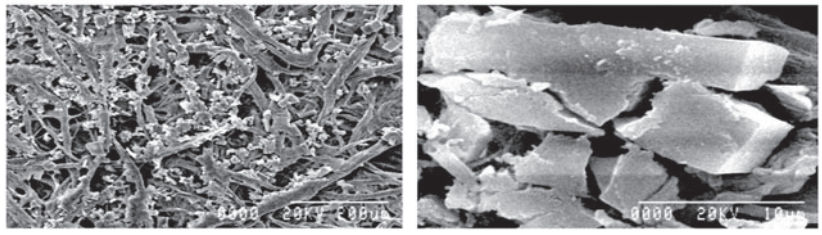

Low resolution High resolution

(b) SEM image of the reduced Hg on the chromatogram

Fig. 1. SEM image of the exchanger (a) SEM image of pure cellulose paper; (b) SEM image of the reduced Hg on the chromatogram.

the cations was found to depend on the composition of the mobile phase system. From chromatogram the R_f values and selectivity factors of the cations with respect to Hg^{+2} were determined. The following important observations have been obtained from the results presented in Tables 2 and 3:

(1) There is no dispersion of metal ions on the developed chromatogram for one component mobile phase system (except 0.05 M HNO_3 where Zn^{+2}, Mn^{+2}, and Bi^{+3} have been dispersed).
(2) Except M_{29}, in all the mobile-phase systems (M_1–M_{28}), either Hg^{+2} becomes dispersed or the selectivity factors were found to be < 1.15 for metal ions with respect to Hg^{+2} indicating a poor separation.
(3) Almost all the metal ions (except Bi^{+3}, Fe^{+3}, Tl^{+3}, and Zr^{+4}) have dispersed in M_{13} (1 M HCl + 20 mL acetone) and M_{19} (0.01 M HNO_3 + 100 mL acetone).
(4) The dispersed area on each chromatogram was extracted in CCl_4 and FTIR studies (Fig. 2) of extracted mass indicated the appearance of a peak at lower range (1602.74 cm^{-1}), which was originally present at a higher frequency at 1622.02–1629.74 cm^{-1} in the spectra of pure CH_3COCH_3. This shifting of the peaks clearly indicates the formation of metal acetone complex on the chromatogram [25]. The formation of kinetics is very fast, and each of these molecules so produced moves with the mobile phase. So, the spots become dispersed on the chromatogram.

3.3. Effect of temperature on the development of the spot on chromatogram

Systematic studies have been made on the development of the spots on the chromatogram using M_{29} as the mobile phase at the range of temperature 290–313 K and plot of log $\left(\frac{V'}{V}\right)$ vs 1,000/T gives a linear relationship ($y = -1267X + 5{,}014$; $R^2 = 1.0$) (Fig. 3).

Where V and V' are volumes of spots on the chromatogram at temperatures T and T', respectively.

The area/volume of the spots was found to increase with the increase in temperature at constant time, analyte character (amount and composition), and character of the stationary and mobile phases. The concentrations of the final states (developed spot) decreased with increase in temperature due to the increased tendencies of diffusion at higher temperatures. The effect of temperature on variation in volumes of spots of Hg^{+2} has been exploited for the determination of the enthalpy change (ΔH) and log K for this diffusion process from the slope ($\frac{\Delta H}{R}$) and intercept (ln K) of Eq. (1) [26], respectively. The analyte (Hg^{+2}) during its forward movement enters alternately into both phases (stationary and mobile) and its behavior is well executed by the temperature-independent parameter K (here, the value of intercept at $\frac{1}{T} = 0$ is the ln K; Fig. 3), the partition constant.

Table 2
Mobility pattern of the metal cations

	R_f values/selectivity factors (α)													
	Mobile phases													
	M_1	M_2	M_3	M_4	M_5	M_6	M_7	M_8	M_9	M_{10}	M_{11}	M_{12}	M_{13}	M_{14}
Hg^{+2}	0.76	0.81	0.90	0.91	0.83	0.90	0.82	0.89	0.88	0.75	0.82	d	d	0.89
Zn^{+2}	0.97 (1.28)	0.97 (1.20)	0.98 (1.09)	0.98 (1.08)	0.92 (1.11)	0.98 (1.08)	0.97 (1.18)	0.98 (1.10)	0.88 (1.00)	d	0.97 (1.18)	0.97	d	0.99 (1.11)
Pb^{+2}	0.85 (1.12)	0.79 (1.03)	0.83 (1.08)	0.79 (1.15)	0.86 (1.04)	0.97 (1.07)	0.90 (1.09)	0.98 (1.10)	0.90 (1.02)	0.83 (1.10)	0.96 (1.17)	d	d	0.76 (1.17)
Cu^{+2}	0.95 (1.25)	0.98 (1.21)	0.99 (1.10)	0.82 (1.11)	0.92 (1.11)	0.97 (1.07)	0.93 (1.13)	0.95 (1.07)	0.32 (2.75)	0.82 (1.09)	0.92 (1.12)	d	d	0.86 (1.03)
Bi^{+3}	0.78 (1.02)	0.95 (1.17)	0.87 (1.03)	0.91 (1.00)	0.85 (1.02)	0.90 (1.00)	0.86 (1.04)	0.89 (1.00)	0.21 (4.19)	d	0.94 (1.14)	0.89 (1.08)	0.91	0.87 (1.02)
Fe^{+3}	0.92 (1.21)	0.92 (1.14)	0.91 (1.01)	0.95 (1.04)	0.89 (1.07)	0.92 (1.02)	0.86 (1.04)	0.93 (1.04)	0.90 (1.02)	0.89 (1.18)	0.94 (1.14)	0.95 (1.02)	0.94 (1.03)	0.90 (1.01)
Mo^{+3}	0.92 (1.21)	0.92 (1.14)	0.98 (1.09)	0.98 (1.08)	0.89 (1.07)	0.89 (1.02)	0.87 (1.06)	0.92 (1.03)	0.10 (8.80)	0.87 (1.16)	0.97 (1.18)	0.98 (1.01)	d	0.88 (1.01)
Tl^{+3}	0.78 (1.02)	0.77 (1.05)	0.77 (1.17)	0.77 (1.18)	0.91 (1.10)	0.81 (1.11)	0.95 (1.15)	0.91 (1.02)	0.85 (1.03)	0.97 (1.29)	0.97 (1.18)	0.76 (1.27)	0.82 (1.10)	0.91 (1.02)
Zr^{+4}	0.95 (1.25)	0.95 (1.17)	0.94 (1.04)	0.97 (1.07)	0.94 (1.13)	0.96 (1.07)	0.94 (1.14)	0.98 (1.10)	0.88 (1.00)	0.89 (1.18)	0.95 (1.15)	0.99 (1.02)	0.95 (1.04)	0.92 (1.03)
Co	0.90 (1.18)	0.97 (1.20)	0.97 (1.08)	0.97 (1.07)	0.94 (1.13)	0.85 (1.06)	0.92 (1.12)	0.94 (1.05)	0.90 (1.02)	0.94 (1.25)	0.92 (1.12)	0.96 (1.01)	d	d
Ni^{+2}	0.95 (1.25)	0.93 (1.15)	0.97 (1.08)	0.95 (1.04)	0.92 (1.11)	0.89 (1.01)	0.93 (1.13)	0.95 (1.06)	0.88 (1.00)	0.97 (1.29)	0.92 (1.12)	d	d	d
Mn^{+2}	0.95 (1.25)	0.96 (1.18)	0.97 (1.08)	0.96 (1.05)	0.91 (1.10)	0.91 (1.01)	0.94 (1.14)	0.97 (1.08)	d	d	0.91 (1.10)	0.98 (1.01)	d	0.99 (1.11)

[d]Dispersed.

Table 3
Mobility pattern of the metal cations (selectivity factors are given in parenthesis)

	R_f values/selectivity factors (α)														
	Mobile phases														
	M15	M16	M17	M18	M19	M20	M21	M22	M23	M24	M25	M26	M27	M28	M29
Hg^{+2}	0.89	0.83	0.87	0.92	D	0.94	0.92	0.94	0.94	0.93	d	d	d	d	0.76
Zn^{+2}	1.0 (1.12)	0.87 (1.04)	d	d	D	0.99 (1.05)	0.95 (1.03)	0.98 (1.04)	0.98 (1.04)		0.97	0.96	d	d	0.98 (1.30)
Pb^{+2}	0.82 (1.08)	0.81 (1.02)	0.80 (1.08)	0.77 (1.19)	0.66	0.92 (1.02)	0.92 (1.00)	0.96 (1.02)	0.96 (1.02)	0.91	0.97 (1.00)	0.95 (1.01)	0.94	0.95	0.05 (15.2)
Cu^{+2}	0.97 (1.08)	0.71 (1.16)	0.65 (1.33)	0.53 (1.73)	0.52 (1.26)	0.95 (1.01)	0.94 (1.02)	0.96 (1.02)	0.97 (1.03)	0.87	0.97 (1.00)	0.97 (1.01)	0.94 (1.00)	0.94 (1.01)	0.93 (1.13)
Bi^{+3}	0.86 (1.03)	d	0.29 (3.00)	0.25 (3.68)	0.05 (13.2)	0.91 (1.03)	0.92 (1.00)	0.94 (1.00)	0.91 (1.03)	0.94	0.92 (1.05)	0.91 (1.05)	0.91 (1.03)	0.90 (1.05)	0.84 (1.10)
Fe^{+3}	1.0 (1.12)	0.87 (1.04)	0.89 (1.02)	0.80 (1.15)	0.75 (1.13)	0.97 (1.03)	0.97 (1.05)	0.97 (1.03)	0.96 (1.02)	0.98	0.98 (1.01)	0.92 (1.04)	0.97 (1.03)	0.98 (1.03)	0.90 (1.20)
Mo^{+3}	d	0.89 (1.07)	0.92 (1.05)	0.98 (1.06)	0.99 (1.50)	0.94 (1.00)	0.95 (1.03)	0.96 (1.02)	0.98 (1.04)		0.98 (1.01)	0.97 (1.01)	0.98 (1.04)	0.97 (1.02)	0.99 (1.30)
Tl^{+3}	0.90 (1.01)		0.91 (1.04)	0.89 (1.03)	0.05 (13.2)	0.87 (1.08)	0.87 (1.05)	0.87 (1.08)	0.91 (1.03)		d	d	d	d	0.71 (1.07)
Zr^{+4}	0.89 (1.00)	0.83 (1.00)	0.90 (1.03)	0.87 (1.05)	0.05 (13.2)	0.96 (1.02)	0.97 (1.05)	0.95 (1.01)	0.95 (1.01)		0.95 (1.02)	0.95 (1.01)	d	0.95 (1.00)	0.98 (1.30)
Co^{+2}	0.93 (1.04)	0.91 (1.09)	0.90 (1.03)	0.85 (1.08)	D	0.96 (1.02)	0.94 (1.02)	0.94 (1.00)	0.93 (1.01)	0.90	0.95 (1.02)	0.95 (1.01)	0.96 (1.02)	0.96 (1.01)	0.95 (1.25)
Ni^{+2}	0.88 (1.01)	0.94 (1.13)	0.88 (1.01)	0.81 (1.13)	D	0.97 (1.03)	0.96 (1.04)	0.85 (1.10)	0.94 (1.00)	0.86	0.97 (1.00)	0.98 (1.02)	0.96 (1.02)	0.96 (1.01)	0.96 (1.26)
Mn^{+2}	1.0 (1.12)	0.84 (1.01)	0.81 (1.07)	d	D	d	0.96 (1.04)	d	d	0.51	d	d	d	d	0.98 (1.30)

[d]Dispersed.

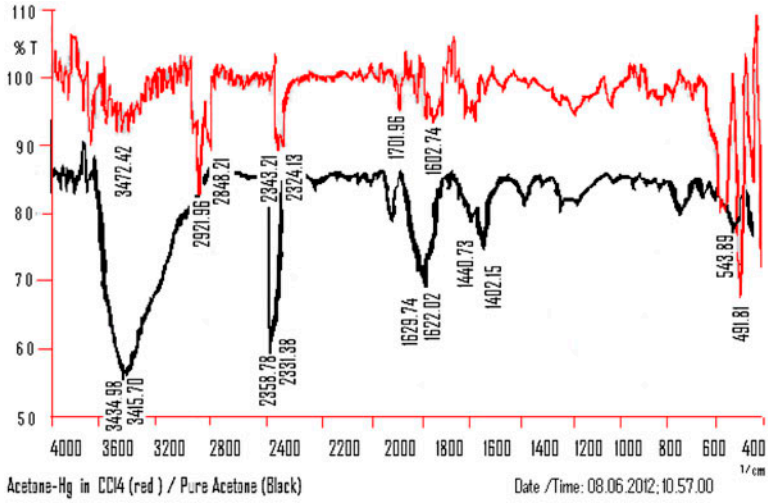

Fig. 2. FTIR spectra of pure acetone and acetone-Hg complex.

$$\ln\left(\frac{V'}{V}\right) = \ln K + \frac{\Delta H}{RT} \quad (1)$$

i.e.

$$\ln\frac{A' \times l}{A \times l} = \ln K + \frac{\Delta H}{RT} \quad (1a)$$

where R is the gas constant = 8.314 J K^{-1} mol^{-1}. A and A' are the initial and final area of the spot, and l is the thickness of the paper strip.

The free energy change (ΔG) and entropy change (ΔS) at room temperature (298 K) were calculated using Eqs. (2) and (3).

$$\Delta G = -2.303\, RT \log K \quad (2)$$

and

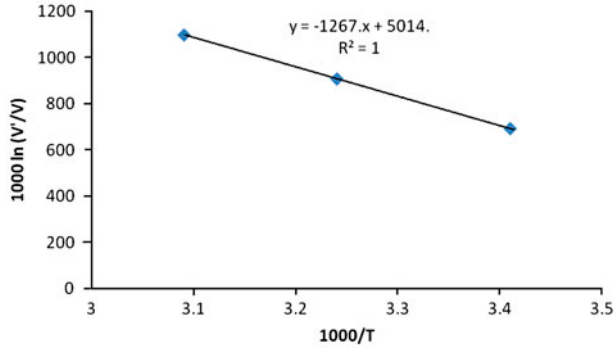

Fig. 3. Plot of log $(\frac{V'}{V})$ vs. 1,000/T.

$$\Delta S = (\Delta H - \Delta G)/T \quad (3)$$

The high equilibrium constant (10^2) and negative ΔH (−10.53 kJ mol^{-1}) indicate the exothermic nature of this liquid–liquid partition process [22], the high negative value of ΔG (−12.52 kJ mol^{-1}) suggests the spontaneity of the process [26], and small positive ΔS (6.63 kJ mol^{-1}) implies that the process is not much disordered but confined to a definite area/volume.

3.4. Interference of foreign ions on R_f values

Systematic studies on R_f values for Hg^{+2} on the developed chromatogram have been made in the presence of foreign ions like of Na^+, K^+, Ca^{+2} and Mg^{+2} in the range concentration 50–400 μg mL^{-1} but considerable interferences were not found (standard deviation = 1.22). These alkali and alkaline earth metal ions on reduction with sodium borohydride produce colorless stains. Thus, even the presence of those ions can not impede the detection of metallic mercury.

3.5. Binary and multicomponent separations

The R_f values and the selectivity factors of metal ions were determined on chromatogram (Tables 2 and 3) using M_{29} as the developing solvent. Result shows that under this recommended condition the lighter metal ions (Zn^{+2}, Cu^{+2}, Fe^{+3}, Mo^{+3}, Zr^{+4}, Mn^{+2}, Co^{+2}, and Ni^{+2}) having molecular mass 55–91, are very weakly bound (R_f value ~0.9), metal ions like Bi^{+3}, Tl^{+3} and Hg^{+2} (molecular mass ~200) are moderately

bound (R_f value 0.7–0.8), while Pb^{+2} is very tightly bound (R_f value <0.05) with the stationary phase. These weakly and moderately bound metal ions are present as $[M(H_2O)]^{+2}$ in 0.1 M acidic condition [27], while Pb^{+2} present as a tetramer, $[Pb_4(OH)_4]^{+4}$. Because of its very high molecular mass, tetrameric Pb^{+2} (~1,000) practically remains unmoved.

In order to assess the possible analytical applications, the proposed method was applied to separate Hg^{+2} from multi-component synthetic mixtures containing Hg^{+2} with different metal ions commonly associated with it in same analytical group, ores and alloy samples. Fifteen difficult and analytically important separations of Hg^{+2} from diverse metal ions in binary and multi-component synthetic mixtures follow the R_f values and selectivity factors (>1.2). Important separations are shown in Fig. 4.

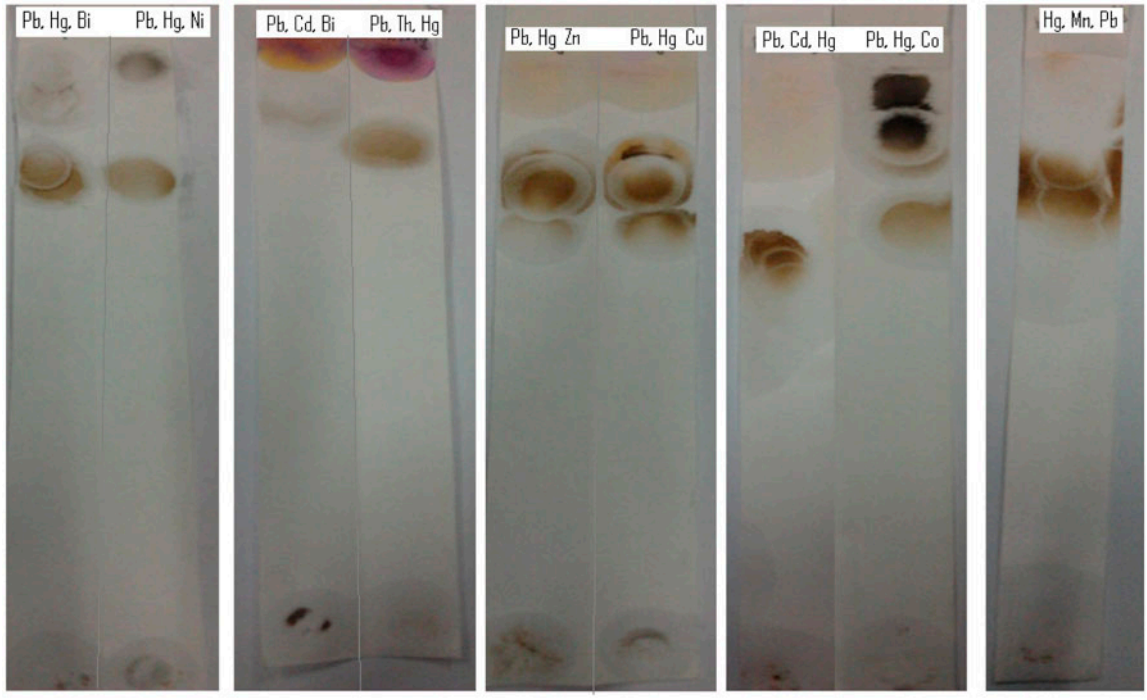

Fig. 4. Chromatogram of multicomponent separations (synthetic samples).

Table 4
Correlation of R_f values of diverse metal ions with their radii and hardness (η_M) values

Metal ions	Radii (pm)	Hardness of metal (η_M) eV	Hardness of exchanger (η_{ex}) eV	$\Delta\eta = (\eta_M - \eta_{ex})$ eV	R_f value
Zn^{+2}	74	10.88	6.34	4.54	0.99
Ni^{+2}	83	8.50		2.16	0.97
Fe^{+3}	79	12.08		5.74	0.94
Co^{+2}	79	8.22		1.88	0.93
Cu^{+2}	87	8.27		1.83	0.93
Zr^{+4}	76	11.25		4.91	0.92
Bi^{+3}	117	3.96		2.38	0.84
Hg^{+2}	116	7.70		1.36	0.76
Tl^{+3}	103	10.40		4.06	0.70
Pb^{+2}	133 ([a]532)	8.46		2.12	0.05

[a]Radii in $[Pb_4(OH)_4]^{+4}$.

3.6. Correlation of R_f value with Desity-Functional (hardness) Index (η)

Whatmann paper contains glucose as the building block of cellulose. The glucose units are stacked one after another one through hydrogen bonding and produce the capillary of radius 500 pm. Metal ions in mobile phase move throgh these capillaries during the chromatographic development. Here, glucose units having O-as binding sites interacted with metal ions according to Pearson's [28], hardness principle. Optimization of the structure of glucose was performed by AMI semi-emperical method. HOMO (−10.7487 eV)—LUMO (1.9266 eV) gap is calculated on the basis of the results obtained using the optimized structure. Utilizing Koopman's theorem (Eq. (4)), the global hardness ($\eta_{ex} = 6.34$ eV) of the glucose unit is determined [29–31]. Among the studied metal ions, Hg^{+2} having closest η (Table 4) should most strongly bind (lowest R_f value) with the glucose unit. With respect to the η values, metal ions like Co^{+2}, Cu^{+2}, Ni^{+2}, Pb^{+2} and Bi^{+3} ($\Delta\eta = 1.88$–2.38 eV) should have the moderate R_f values. Due to higher differences in η values ($\Delta\eta = 4.06$–5.74 eV), metal ions like Tl^{+3}, Zn^{+2}, Zr^{+4} and, Fe^{+3} should be placed at topper end on the developed chromatogram. But, the order is not regular probably the solvated metal ions do not interact with their absolute hardness (η_M). Regarding the radii of metal ions and exchanger site, Co^{+2}, Cu^{+2}, Ni^{+2}, Fe^{+3} and Zn^{+2} ($r = 0.69$–0.88 pm) should passes through the cellulose pore with higher mobility ,while Pb^{+2} in its tetrameric form ($r = 532$ pm) having highest radii (and

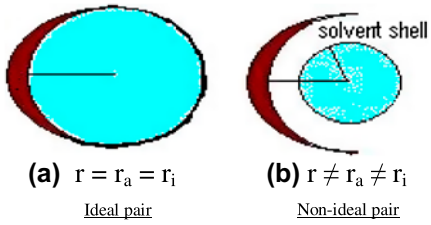

Fig. 5. Interaction pattern of acid–base pair.

Table 5
Correlation of R_f values of diverse metal ions with corrected hardness (η^*_M) values (values for oxo-species are given in parenthesis)

Metal ions	$(\delta) = [1-(r/r_i)]$	$\eta^* = \eta - \eta \times \delta$ (eV)	$\Delta\eta_c = (\eta^*_M - \eta_{ex})$ (eV)	R_f value
Zn^{+2}	0.88	1.30	5.04	0.99
Ni^{+2}	0.86	1.19	5.15	0.97
Fe^{+3}	0.86	1.69	4.65	0.94
Co^{+2}	0.87	1.07	5.27	0.93
Cu^{+2}	0.86	1.20	5.14	0.93
Zr^{+4}	0.84	1.57	4.76	0.92
Bi^{+3}	0.77 (0.51)	0.91 (1.94)	5.43 (4.40)	0.84
Hg^{+2}	0.80	1.54	4.80	0.76
Tl^{+3}	0.83	1.77	4.57	0.70
Pb^{+2}	0.77	1.95	4.39	0.05

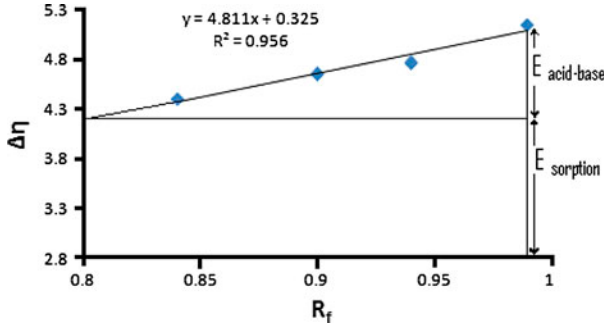

Fig. 6. Plot of R_f values vs. $\Delta\eta$.

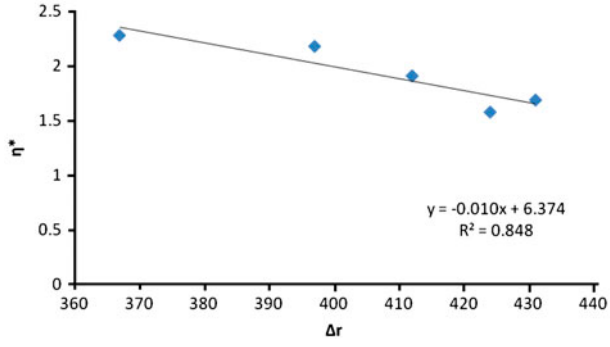

Fig. 7. Plot of δr vs. η^*.

Table 6
Overview of hydrated radii, correlation of calculated values with literature values [23]

Metal ions	η^*	Hydrated radii (calculated) pm	Hydrated radii (literature values) pm
Zn^{+2}	1.30 (1.25)[a]	553.7 (575.9)[a]	600
Ni^{+2}	1.18	610.0	600
Fe^{+3}	1.69 (1.16)[a]	425.9 (620.5)[a]	600
Co^{+2}	1.07	672.7	600
Cu^{+2}	1.20	599.9	600
Zr^{+4}	1.57	459.0	1,100
Bi^{+3}	1.58	470.0	–
Hg^{+2}	1.46	493.0	500
Tl^{+3}	1.79	402.1	–
Pb^{+2}	1.94 (1.70)[a]	371.0 (423.4)[a]	590

[a]Values obtained from plot are given in parenthesis.

greater than pore radii, 500 pm) should remain unmoved. And metal ions like Tl^{+3}, Hg^{+2}, and Bi^{+3} ($r = 1.03$–1.17 pm) should have the moderate mobility. Thus, the radius factor plays an anchoring role on the movement (R_f value) of the metal ions on the chromatogram.

$$\eta = \frac{1}{2}\{\varepsilon_{LUMO} - \varepsilon_{HOMO}\} \quad (4)$$

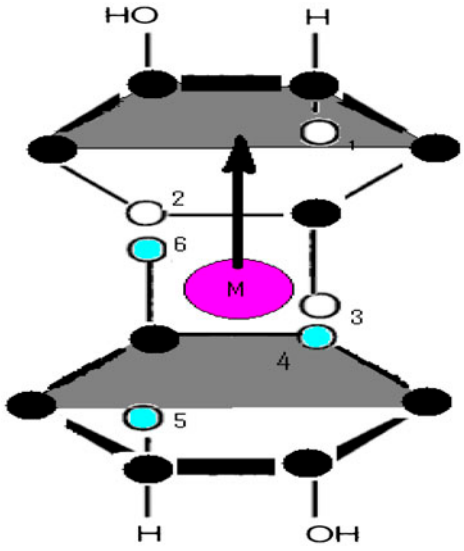

Fig. 8. Probable attachment of metal ions into the glucose moities during equlibration. The shaded area represents the back side of the ring.

3.7. Correlation of R_f value with corrected hardness (η^*)

Radii of the metal ions are very much smaller (<120 pm) than the core radius of glucose ring (500 pm). During equilibration, a definite solvent shell exists in between the metal ion and glucose ring as per following suggested path (Fig. 5(b)). Hardness of the hydrated metal ion depends on the aggregation of water shell with the metal ion and may be represented by Ghosh et al. additivity formula [32], or by Dutta's product formula [33].

Thus, the operative hardness of diverse ions for Pearson acid–base interaction [24] would differ from their absolute values. In this case, the relative deviation (δ) of the radii ratio (i.e. $\delta = 1 - r/r_i$; Where r is the radii of any metal ion under consideration, r_i [ideal radii] is the radii of the glucose core) is an index of proximity of acid–base pair with respect to η and which in turn reflects the closeness between the absolute radii and solvated ionic radii. Mathematically, as $r \to r_i$, r_s (solvated radius) $\to r_a$ (absolute radius), $\delta \to 0$ and so, $\eta^* \to \eta$ Eq. (5). With the decrease in the δ value, the acid–base pair will come closer to introduce the better acid–base interaction. At a limiting value of $\delta = 0$ (i.e. when $r_i = r$) the closeness of the acid–base pair is highest, and thus, interaction is highest with almost 100% of their absolute hardness values. Based on the above argument, the working empirical formula for the calculation of corrected hardness (η^*) for the metal ions could be proposed as:

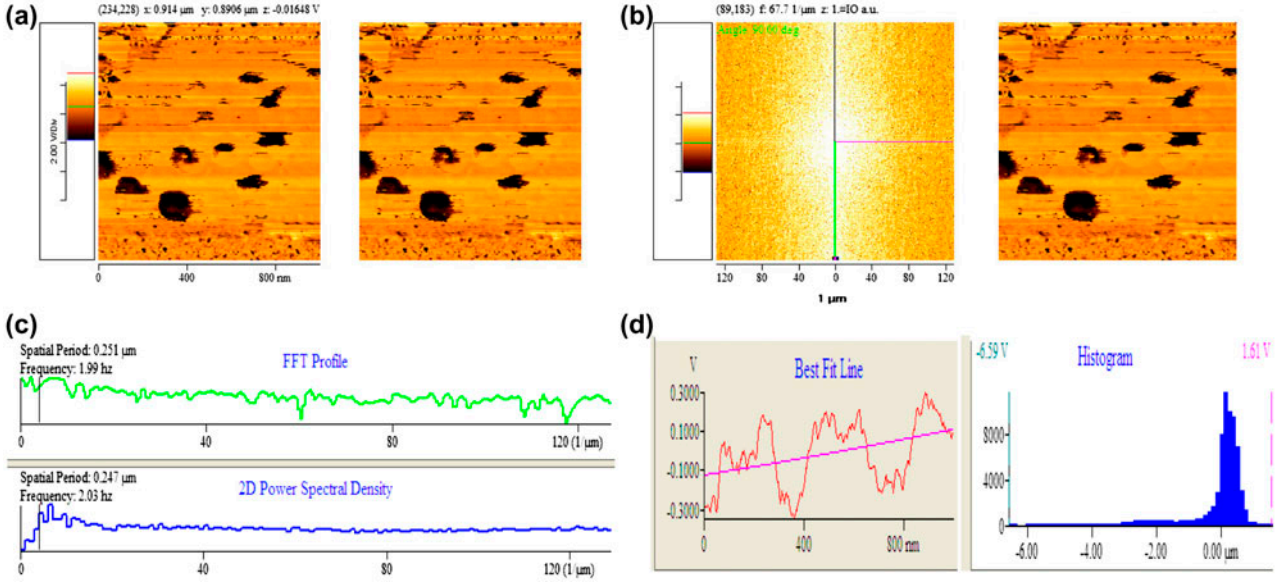

Fig. 9. AFM image of developed chromatogram after borohydride reduction. (a) Diposition pattern of Hg and (b) diposition pattern at high resolution (c) FFT profile (d) height profile of (a & b).

Table 7
Separation of Hg^{+2} from real samples

Sample		Separation parameters				
		Sl. no	Metal ion (added)	[a]R_f values (cm)	Selectivity factors (α)	Standard deviation
Blood samples	Blood serum	1.	Hg^{+2}	0.68		0.12
			Pb	0.04	17.0	0.08
			Zn	0.99	1.45	0.22
		2.	Hg	0.70		0.31
			Pb	0.04	17.5	0.09
			Cu	0.99	1.41	0.07
		3.	Hg	0.70		0.08
			Pb	0.05	14.0	0.24
			Bi	0.97	1.39	0.26
		4.	Hg	0.70		0.09
			Pb	0.05	14.0	0.42
			Cd	0.98	1.40	0.08
		5.	Hg	0.73		0.22
			Pb	0.05	14.6	0.23
			Ni	0.97	1.33	0.26
Raw water		1.	Hg	0.78		0.32
			Pb	0.04	19.5	0.22
			Ni	0.95	1.22	0.18
		2.	Hg	0.78		0.16
			Pb	0.04	19.5	0.33
			Bi	0.94	1.21	0.08
		3.	Hg	0.75		0.16
			Pb	0.04	18.75	0.28
			Cd	0.97	1.29	0.25
		4.	Hg	0.74		0.32
			Pb	0.04	18.5	0.41
			Zn	0.99	1.34	0.08
		5.	Hg	0.75		0.16
			Pb	0.04	18.75	0.08
			Cu	0.95	1.27	0.26
		6.	Pb	0.04	17.5	0.14
			Cd	0.97	1.39	0.08
			Tl	0.70		0.22
		7.	Hg	0.75		0.32
			Pb	0.04	18.75	0.18
			Co	0.93	1.24	0.26
Distilled water		1.	Hg	0.75		0.16
			Pb	0.04	18.75	0.06
			Mn	0.99	1.32	0.08
		2.	Hg	0.79		0.18
			Pb	0.04	19.75	0.24
			Th	0.98	1.24	0.28
		3.	Tl	0.80		0.44
			Pb	0.04	20.0	0.18
			Co	0.98	1.23	0.08

(*Continued*)

Table 7
(*Continued*)

Sample	Separation parameters				
	Sl. no	Metal ion (added)	[a]R_f values (cm)	Selectivity factors (α)	Standard deviation
	4.	Tl	0.75		0.14
		Pb	0.04	18.75	0.12
		Ni	0.92	1.23	0.22
	5.	Tl	0.74		0.32
		Pb	0.04	18.5	0.29
		Cu	0.94	1.27	0.18
	6.	Tl	0.70		0.18
		Pb	0.04	17.5	0.22
		Bi	0.87	1.24	0.09
	7.	Tl	0.70		0.16
		Pb	0.04	17.5	0.32
		Fe	0.94	1.34	0.08
	8.	Tl	0.71		0.18
		Pb	0.04	17.75	0.22
		Zn	0.99	1.39	0.31
	9.	Tl	0.75		0.28
		Pb	0.04	18.75	0.16
		Mn	0.97	1.29	0.09
	10.	Bi	0.85		0.28
		Pb	0.04	21.25	0.14
		Mn	0.97	1.14	0.22
	11.	Tl	0.75		0.12
		Pb	0.04	18.75	0.33
		Cd	0.99	1.32	0.41
	12.	Bi	0.86		0.16
		Pb	0.04	21.50	0.09
		Cd	0.99	1.15	0.18
	13.	Bi	0.88		0.32
		Pb	0.04	22.00	0.18
		Th	0.99	1.12	0.26
	14.	Tl	0.85		0.06
		Pb	0.04	21.25	0.18
		Th	0.99	1.16	0.32

[a]Average of five determinations.

$$\text{Relative deviation}(\delta) = [1 - (r/r_i)];\ \text{and}\ \eta^* = \eta - \eta\,\delta \quad (5)$$

Thus, when, $\delta = 0$, (at $r_i = r$), $\eta^* = \eta$; metal ions having ideal radius interacts with their absolute hardness with the exchanger.

The corrected hardness, η^* has been determined (Table 5) from the empirical formula. In terms of hardness, Pb^{+2} and the binding site of the exchanger match best (i.e. smallest $\Delta\eta$) and Pb^{+2} is tightly bound (lowest R_f value). Metal ions with higher $\Delta\eta$ values are loosely bound and placed at the topper end of the chromatogram. While moderately bound metal ions ($\Delta\eta = 4.60 \pm 0.2$) are placed at the middle part of the chromatogram. Probably, the oxo-species of Bi^{+3} and Zr^{+4} have different radii value and show their anomalous behavior.

3.8. Sorption energy and acid base binding energy

Plot of R_f values vs. $\Delta\eta$ ($=\eta_{ex} - \eta^*$) gives a linear plot (Fig. 5) ($y = 4.811x + 0.325$; $R^2 = 0.956$) with an intercept of 0.325. At $x = 0$ (i.e. $R_f = 0$), exchanger—metal

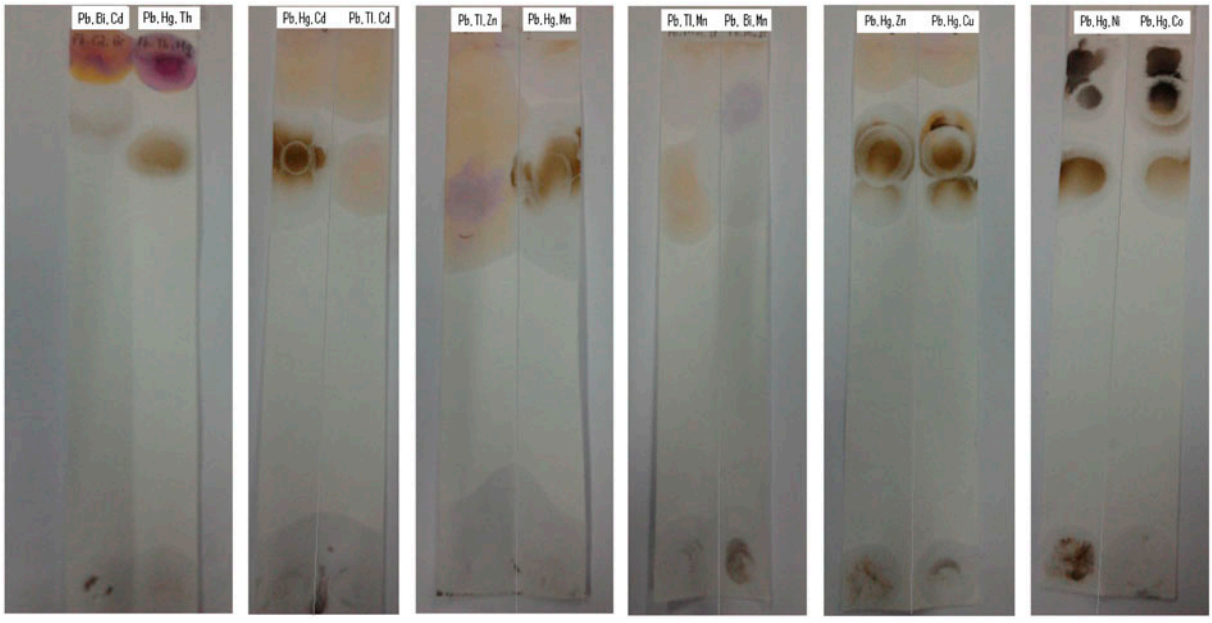

Fig. 10. 12 important ternary separations from blood samples.

binding becomes maximum, and $\Delta\eta$ should become zero [28]. But, at $x = 0$; $\Delta\eta = 0.325$ eV (Fig. 6) indicating that at this recommended condition, exchanger—metal is not perfectly bound, and metal ion should be in motion with an equivalent value of energy 0.325 eV. So, acid–base interaction behavior is not the sole factor so far as the movement of the metal ions is concerned. And, due to some sort of sorption behavior (act in opposite direction) it remains unmoved ($R_f = 0$) with a threshold energy (sorption) of 0.325 eV (31.3 kJ mol^{-1}) and agreed well with literature values (45.67–68.72 kJ mol^{-1} for the sorption of bivalent ions on single walled carbon nanotube having o-binding site) [34]. At $x = 1$ (i.e. $R_f = 1$), $\Delta\eta = 5.136$ eV is the amount of total energy ($E_{\text{sorption}} + E_{\text{acid–base}}$) required for free movement of metal ions. The slope is the desorption tendency ($K_{\text{desorption}}$) with a constant value of 0.048×10^2. Here, $E_{\text{acid–base}}$ is a function of movement of metal ions (R_f values) on the chromatogram.

3.9. Determination of hydrated radii from corrected hardness (η^*)

The Eq. (5) can be represented as:

$$\eta^* = \eta - \eta \times (r_i - r)/r_i; \text{i.e.} \eta^* = \eta - \eta \times \Delta r/r_i \quad (6)$$

where Δr represent the solvent shell as per Fig. 5.

Thus, there is a linear relationship between Δr and η^*. Plot of Δr (difference between solvated radii and absolute radii of metal ion, $r_s - r_a$) vs. η^* gives a linear plot ($y = -0.010x + 6.374$) with an intercept of 6.374 (Fig. 7). Here, the variation of Δr has been made by changing radii of the metal ion. At $\Delta r = 0$, solvated radii is equal to absolute radii (Fig. 5) and at this recommended condition, η^* should approach to η (absolute hardness). From the corrected η^*, the hydrated radii of the metal ions have been determined by the following relationship (Eq. (7)), and these calculated values (Table 6) agreed well with the Kiland values [23],

$$\eta = 1/2r \quad (7)$$

where η = hardness and r = radii.

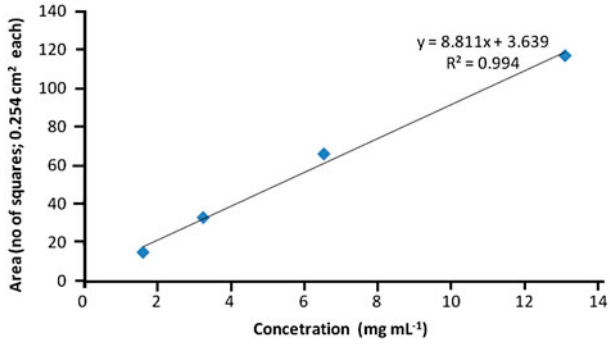

Fig. 11. Plot of concentration (mg mL^{-1}) vs. area (no of squares; each of 0.154 cm^2).

3.10. Probable mechanistic path

The morphological characters and sizes of diposited Hg on the chromatogram were determined by SEM and atomic force microscopy (AFM, VEECO, dicpII). Solvated metal ions moves through the micro capillaries so produced by the stacking of glucose molecules one after another one as per the probable mechanistic path (Fig. 8). During the movement metal ions that which are present in between the two glucose rings, interact through hard-soft nature of binding with the oxygen sites (1, 2, 3 of one glucose ring and 4, 5, 6 of the second glucose ring) of the exchanger. Generally, metal ions are of lower in size in comparison with the capillari size. In such cases, the solvent core that is present in between the metal ion and exchange site is dragging the ions and keeps them in motion. Differential migration of the ions correlates with the variation in solvent (mobile phase) core for the diverse ions. High-resolution AFM images of the chromatogram also unambiguously confirm the discontinuous diposition of Hg (Fig. 9(a) and (d)) and supports the probable mechanistic path.

3.11. Separation of mercury from real samples

The effectiveness of the proposed method was judged by separating Hg^{+2} from raw water (well, pond, and tap) samples. The feasibility of the process was tested by separating Hg^{+2} from human blood samples containing diverse congeners for its serological sample analysis. Results are given in Table 7. And the separation profiles are given in Fig. 10.

3.12. Estimation of unknown concentration of Hg(II)

Systematic studies have been made on area of the spot on chromatogram at the range of concentration 13.1–3.275 mg mL^{-1} of Hg(II). The developed area on the chromatogram was measured and plot of concentration vs. area generates a straight line ($y = 8.811x + 3.639$; $R^2 = 0.994$) (Fig. 11). The concentration of an unknown analyte was determined from the plot. The values (synthetic solution: 4.38; raw water: 4.52; and tap water: 4.48 mg mL^{-1}) are compatible (relative error: 1.60 ± 0.66 and relative standard deviation: 2.63 $\pm$ 0.46) with standard values (4.42 mg mL^{-1}) obtained complexometrically [35].

4. Conclusions

The proposed borohydride reduction method for metal ion detection on chromatogram is simple, rapid, selective, eco-friendly, and cost-effective. Alkali and alkaline earths do not interfere the detection of Hg(II) by borohydride reduction on the chromatogram. Clean separations ($\alpha \geqslant 1.21$) of Hg(II) have been achieved from several toxic and heavy metal ions like Pb(II), Fe (III), Cu(II), Zn(II), Ni(II), Bi(III), Tl(III), Zr(IV), and Cd (II) in synthetic multicomponent mixtures. Clean separation of Hg(II) has also been achieved from blood serum and platelets containing chemical congeners which appear to be highly applicable to forensic serological and toxicological analysis. Sorption energy, acid-base-binding energy and hydrated radii have been determined from Density Functional (hardness) Index and their values agree well with the literature values.

Acknowledgments

The authors wish to thank UGC-SAP, New Delhi, India and Department of Chemistry, Visva-Bharati, Santiniketan, India for financial support.

References

[1] N.J. Modi, Modi's Text Book of Medical Jurisprudence and Toxicology, 20th ed., N. M. Tripathi Pvt. Ltd., Bookshellers, Mumbai, 1977.
[2] WHO, Environmental Health Criteria 86. Mercury—Environmental Aspects, World Health Organization, Geneva, 1989.
[3] Encyclopedia Britannica Yearbook, Yearbook of Science and the Future, March, 1980.
[4] O. Lindquist, A. Jernelov, K. Johannson, R. Rodhe, Mercury in the Swedish Environment, National, 1984. Global and local sources, report 1816, National Swedish Environmental Protection Agency, Stockholm, 121. As cited by von Rein and Hylander (2000).
[5] M. Morita, J. Yoshinaga, J.S. Edmonds, The determination of mercury species in environmental and biological samples (technical report), Pure Appl. Chem. 70(8) (1998) 1585–1615.
[6] C.E. Oda, J.D. Ingle, Continuous flow cold vapor atomic absorption determination of mercury, Anal. Chem. 53 (1981) 2030–2033.
[7] M.J. Low, J.C. Wei, S. Yeh, Preconcentration of mercury, gold and copper in sea water with lead dithiocarbamate for neutron activation, J. Anal. Chem. 49 (1977) 1146–1150.
[8] T. Nedeltcheva, L. Kostadinova, N. Elenkova, M. Attannesova, K. Mineva, Determination of copper and cadmium trace elements in phosphates in stripping voltametry, Anal. Lab. 3 (1994) 102–104.
[9] M. Tsubonchi, Spectrophotometric determination of trace amounts of mercury (II), Anal. Chem. 42 (1970) 1087–1090.
[10] R.E. Mansell, E. Hunemorder, A photometric method for trace determination using Beckman, DU spectrophotometer, J. Anal. Chem. 35 (1963) 1981–1981.
[11] A. Ciucci, M. Corsi, V. Palleschi, S. Rastelli, A. Salvetti, E. Tognoni, New procedures for quantitative elemental analysis by laser-induced plasma spectroscopy, Appl. Spectrosc. 53 (1999) 960–964.
[12] B. Mandal, U.S. Roy, D. Datta, N. Ghosh, Combined cation-exchange and extraction chromatographic method of pre-concentration and concomitant separation of Cu(II) with high molecular mass liquid cation exchanger after its online detection, J. Chromatogr. A 1218 (2011) 5644–5652.
[13] B. Mandal, N. Ghosh, Combined cation-exchange and extraction chromatographic method of pre-concentration and concomitant separation of bismuth(III) with high molecular mass liquid cation exchanger, J. Hazard. Mater. 182 (2010) 363–370.

[14] B. Mandal, N. Ghosh, Extraction chromatographic method of preconcentration and separation of lead (II) with high molecular mass liquid cation exchanger, Desalination 250 (2010) 506–514.
[15] L. Carrasco, S. Díez, J.M. Bayona, Simultaneous determination of methyl- and ethyl-mercury by solid-phase microextraction followed by gas chromatography atomic fluorescence detection, J. Chromatogr. A 1216 (2009) 8828–8834.
[16] S.N. Tewari, Analysis of inorganic compounds by paper chromatography: The separation and detection Of Cu, Ni, Co, Hg, Ag and Pb, Colloid Polym. Sci. 135 (1954) 159–160.
[17] N.N. Hemanand, N.V. Nanda Kumar, Detection of compounds of mercury, cadmium and copper by baker's dry yeast enzyme inhibition, MEJSR 6(2) (2010) 152–156.
[18] J.N. Bartlett, G.W. Curtis, Paper chromatography of organic mercury compounds, Anal. Chem. 34(1) (1962) 80–82.
[19] M. Qureshi, M.A. Khan, Fast paper chromatography of different valence states of mercury and antimony, Anal. Chem. 35 (13) (1963) 2050–2052.
[20] J.G. Dorsey, Solvatochromic investigation of chromatographic retention mechanisms, J. Chromatogr. A 2(5) (1987) 37–41.
[21] A.J.P. Martin, R.L.M. Synge, A new form of chromatogram employing two liquid phases, Biochem. J. 35 (1941) 1357–1368.
[22] J.J.V. Deemter, F.J. Zuiderweg, A. Klinkenberg, Longitudinal diffusion and resistance to mass transfer as causes of nonideality in chromatography, Chem. Eng. Sci. 5 (1956) 271–289.
[23] J. Kielland, Activity coefficients of ions in aqueous solutions, J. Am. Chem. Soc. 59 (1937) 1675–1678.
[24] R.G. Pearson, Hard and soft acids and bases, J. Am. Chem. Soc. 85 (1963) 3533–3543.
[25] K. Nakamoto, Infrared and Raman Spectra of Inorganic and Coordination Compounds, Part B, 5th ed., (John Wiley). pp. 59–61 1977.
[26] P. Atkins, J. Paula, Atkins' Physical Chemistry, International Student Edition, 8th ed., Oxford University Press, Oxford, 2006, pp. 77–117.
[27] F.A. Cotton, G. Wilkinson, Advanced Inorganic Chemistry, 5th ed., John Wiley, New York, NY,. pp. 175–380, 598–607, 692–920 1998.
[28] R.G. Pearson, Acids and bases, Science 151 (1966) 172–177.
[29] R.S. Muliken, Molecular compounds and their spectra, J. Am. Chem. Soc. 74 (1952) 811–824.
[30] R.G. Pearson, Hard and Soft Acids and Bases, Dowden (Ed.), Hutchinson and Ross, Stroudsville, PA, 1973.
[31] R.G. Pearson, Absolute electronegativity and hardness: Application to inorganic chemistry, Inorg. Chem. 27 (1988) 734–740.
[32] W. Yang, C. Lee, S.K. Ghosh, Molecular softness as the average of atomic softnesses: Companion principle to the geometric mean principle for electronegativity equalization, J. Phys. Chem. 89 (1985) 5412–5415.
[33] D. Dutta, Geometric mean principle for hardness equalization, a corollary of Sanderson's geometric mean principle of electronegativity equalization, J. Phys. Chem. 90 (1986) 4216–4217.
[34] O. Moradi, K. Zare, M. Yari, Interaction of some heavy metal ions with single walled carbon nanotube, Int. J. Nano Dim. 1(3) (2011) 203–220.
[35] I. Persson, Hydrated metal ions in aqueous solution: How regular are their structures? Pure Appl. Chem. 82(10) (2010) 1901–1917.